Dalton Transactions

Cite this: *Dalton Trans.*, 2012, **41**, 8913

www.rsc.org/dalton

PAPER

UV-vis-NIR and EPR characterisation of the redox series $[MQ_3]^{2+,+,0,-,2-}$, M = Ru or Os, and Q = *o*-quinone derivative†

Atanu Kumar Das,[a] Ralph Hübner,[a] Biprajit Sarkar,[a] Jan Fiedler,[b] Stanislav Záliš,[b] Goutam Kumar Lahiri[c] and Wolfgang Kaim*[a]

Received 18th April 2012, Accepted 22nd May 2012
DOI: 10.1039/c2dt30846k

The neutral title compounds with Q = 3,5-di-*tert*-butyl-*o*-quinone or 4,6-di-*tert*-butyl-*N*-phenyl-*o*-iminobenzoquinone (Q_x) were studied by UV-vis-NIR spectroelectrochemistry and by EPR spectroscopy in the case of the odd-electron monocation and monoanion intermediates. Supported by DFT and TD-DFT calculations, the results indicate stepwise electron removal from predominantly ligand-based delocalised MOs on oxidation whereas the stepwise electron uptake on reduction involves unoccupied MOs with considerably metal–ligand mixed character. In both cases, the strong near-infrared absorption of the neutral precursors diminishes. In comparison to the ruthenium series, the osmium analogues exhibit larger transition energies from enhanced MO splitting and a different EPR response due to the higher spin–orbit coupling. The main difference between the quinone (**1″**, **2″**) and corresponding monoiminoquinone systems (**3″**, **4″**) is the shift of about 0.6 V to lower potentials for the monoimino analogues. While the absorption features do not differ markedly, the EPR data reflect a higher degree of covalent bonding for the complexes with monoimino ligands.

Introduction

The noninnocence[1] of 1,2-dioxolene ligands with their *o*-quinone, *o*-semiquinone and catecholate redox forms has provided some challenging problems regarding the most appropriate assignments of oxidation states in corresponding transition metal complexes.[2] In addition to 1 : 1 metal–dioxolene ligand complexes,[3] the tris-ligand compounds $[MQ_3]^n$ have received much attention,[4,5] and various oxidation state assignment alternatives were thus proposed. With group 8 metals and the standard ligand, strategically protected Q = 3,5-di-*tert*-butyl-*o*-quinone, the work reviewed by Pierpont and coworkers[2] suggested that the FeQ_3 system involves high-spin iron(III) and semiquinone ligands[4c] whereas the structure analysis[5] of diamagnetic OsQ_3 indicated a "slightly more catechol-like" situation which would imply osmium(VI). The similarly diamagnetic RuQ_3 (*cis*- and *trans*-forms due to the asymmetry of Q) was described as exhibiting bond lengths that are "more semiquinone-like",[5] however, the "detailed features….are consistent with neither semiquinonate nor catecholate charge formulations for the ligands".[5] Differences between the electronic structures of RuQ_3 and OsQ_3 were noted in the form of different dynamic behaviour on the NMR time scale, with rigidity observed for the ruthenium system but fluxionality of the osmium analogue.[5] Since ruthenium compounds with *o*-quinonoid ligands have generally been shown to involve intricate electronic structures due to mixing of metal- and ligand-based frontier orbitals,[6–8] we have probed the complexes RuQ_3 (**1**), OsQ_3 (**2**), $Ru(Q_x)_3$ (**3**),[6] and the new $Os(Q_x)_3$ (**4**), Q_x = 4,6-di-*tert*-butyl-*N*-phenyl-*o*-iminobenzoquinone, with the aim of establishing the electronic configuration in the accessible oxidised and reduced forms, using EPR and UV-vis-NIR spectroelectrochemistry and supporting TD-DFT calculations.

While ruthenium complexes containing Q have received attention in relation to catalytic processes like water oxidation,[9] the $Q_x^{0/\cdot-/2-}$ series has been much employed as a ligand redox system in coordination chemistry.[1c,6,10] Its mixed O/NPh hybrid coordination helps to avoid both the poor basicity and thus enhanced dissociation of quinones as well as the strong nucleophilicity and orbital mixing of the *o*-quinonediimine/*o*-phenylenediamido(2−) system.[7b] Tris(chelate) metal complexes such as MQ_3 or the much studied[9] $[Ru(bpy)_3]^{2+}$ provide a challenge for theory because of orbital[11] degeneracy resulting from trigonal symmetry.

[a]*Institut für Anorganische Chemie, Universität Stuttgart, Pfaffenwaldring 55, D-70550 Stuttgart, Germany*
[b]*J. Heyrovský Institute of Physical Chemistry, v.v.i., Academy of Sciences of the Czech Republic, Dolejškova 3, CZ-18223 Prague, Czech Republic*
[c]*Department of Chemistry, Indian Institute of Technology Bombay, Powai, Mumbai-400076, India*

†Electronic supplementary information (ESI) available: DFT calculated structure data of **1** and **2** (Table S1), Table S2 (bond angles in **4**), cyclic voltammograms of **1**, **2** and **4** (Fig. S1), EPR spectra of $\mathbf{2}^+$ and $\mathbf{1}^-$ (Fig. S2, S3), frontier MO representations of **1** (Fig. S4), and spectroelectrochemical response of **4** (Fig. S5). CCDC 876432. For ESI and crystallographic data in CIF or other electronic format see DOI: 10.1039/c2dt30846k

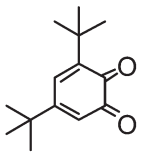

Q

3,5-di-*tert*-butyl-*o*-benzoquinone

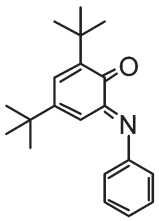

Q_x

4,6-di-*tert*-butyl-*N*-phenyl-*o*-iminobenzoquinone

Experimental methods

Instrumentation

EPR spectra in the X band were recorded with a Bruker System EMX. UV-vis-NIR absorption spectra were recorded on J&M TIDAS and Shimadzu UV 3101 PC spectrophotometers. Cyclic voltammetry was carried out in 0.1 M Bu_4NPF_6 solutions using a three-electrode configuration (glassy carbon working electrode, Pt counter electrode, Ag/AgCl reference electrode) and a PAR 273 potentiostat and function generator. The ferrocene/ferrocenium (Fc/Fc^+) couple served as an internal reference. Spectroelectrochemistry was performed using an optically transparent thin-layer electrode (OTTLE) cell.[12] A two-electrode capillary served to generate intermediates for X band EPR studies.[13]

The compounds **1** and **2** were obtained as described,[5] complex **3** has been fully characterised.[6]

Synthesis of $Os(Q_x)_3$ 4. Compound **4** was obtained in analogy to **3**,[6] by reacting the metal(III) chloride with H_2Q_x under basic conditions for 6 h in acetonitrile (yield: 50%). Anal. Calcd for $C_{60}H_{75}N_3O_3Os$ (M = 1076.49 g mol^{-1}): C, 66.94; H, 7.02; N, 3.90%. Found: C, 67.08; H, 7.12; N, 3.82%. MS (ESI) Calcd for $C_{60}H_{75}N_3O_3Os$ ($[M + H]^+$): *m/z* = 1078.55; found 1078.55. ^{1}H-NMR (acetone-d_6): 7.14 (b, 9H), 6.81 (b, 3H), 6.67 (b, 4H), 6.47 (b, 5H), 1.24 (s, 18H, $(C(CH_3)_3)$), 1.09 (s, 18H, $(C(CH_3)_3)$).

Crystallography

Single crystals were obtained by diffusion of CH_3CN into a dichloromethane solution of **4**. Compounds **3**[6] and **4** crystallise isostructurally. Data for the new **4**: empirical formula $C_{60}H_{75}N_3O_3Os$; M_r = 1076.43; T = 100(1) K, λ = 0.71073 Å; orthorhombic, space group $P2_12_12_1$; a = 13.0545(1), b = 17.3817(2), c = 23.3892(3) Å; V = 5307.2(2) Å^3; Z = 4; $F(000)$ = 2224; D = 1.347 g cm^{-3}; μ = 2.449 mm^{-1}; 2θ = 1.46–26.72°; $-31 \leq h \geq 29$, $-12 \leq k \geq 0$, $0 \leq l \geq 27$; 11 233 indep. reflections; data/restraints/parameters 10 526/0/604; $R[F^2 > 2\sigma(F^2)]$ = 0.0522; w$R(F^2)$ = 0.0538; GOF = 1.019; R_{int} = 0.0271; R_{all} = 0.0325; $\Delta\sigma_{max}$, $\Delta\sigma_{min}$: 0.969; −1.124 e A^{-3}. X-ray diffraction data were collected using a Nonius Kappa CCD single-crystal X-ray diffractometer. The structures were solved and refined by full-matrix least-squares techniques on F^2 using the SHELX-97 programme.[14] The absorption corrections were done using the multiscan technique. All data were corrected for Lorentz and polarisation effects, and the non-hydrogen atoms were refined anisotropically. Hydrogen atoms were included in the refinement process as per the riding model.

DFT calculations

The geometrical and electronic structures of **1** and **2** were calculated by the density functional theory (DFT) method using the Gaussian 03[15] and ADF2010.01[16] program packages on experimental structures. Electronic transitions were calculated by the time-dependent DFT (TD-DFT) method.

The hybrid functional of Perdew, Burke and Ernzerhof[17] (PBEO) was used within Gaussian (G03/PBE0) together with 6-31G* polarised double-ζ basis sets[18] for C, H, N and O atoms and effective core pseudopotentials and corresponding optimised sets of basis functions for the Ru and Os atoms.[19] The solvent was described by the polarisable conductor calculation model (CPCM)[20] in TD-DFT calculations.

Slater type orbital (STO) basis sets of triple-ζ quality with two polarisation functions for the Ru and Os atoms and of triple-ζ quality with one polarisation function for the remaining atoms were employed within ADF. The inner shells were represented by the frozen core approximation (1s for C, N, O, 1s–3d for Ru and 1s–4d for Os were kept frozen). The calculations were done with the functional including Becke's gradient correction to the local exchange expression in conjunction with Perdew's gradient correction to the local correlation (ADF/BP).[21] The scalar relativistic (SR) zero order regular approximation (ZORA) was used within ADF calculations. The *g* tensor was obtained from a spin-nonpolarised wave function after incorporating the spin–orbit (SO) coupling. *A* and *g* tensors were obtained by first-order perturbation theory from a ZORA Hamiltonian in the presence of a time-independent magnetic field.[22] Core electrons were included in calculations of *A* tensors.

Results and discussion

Complexes **1** and **2** were prepared according to literature procedures.[5] The reported structural parameters of **1** and **2** were well reproduced by DFT (Table S1†). The diamagnetism, illustrated through narrow ^{1}H-NMR lines, was attributed[5] to strong antiferromagnetic spin–spin coupling. Like the analogous **3**,[6] the new compound **4** exhibits corresponding behaviour. The compounds **3**[6] and **4** crystallise isostructurally with meridional

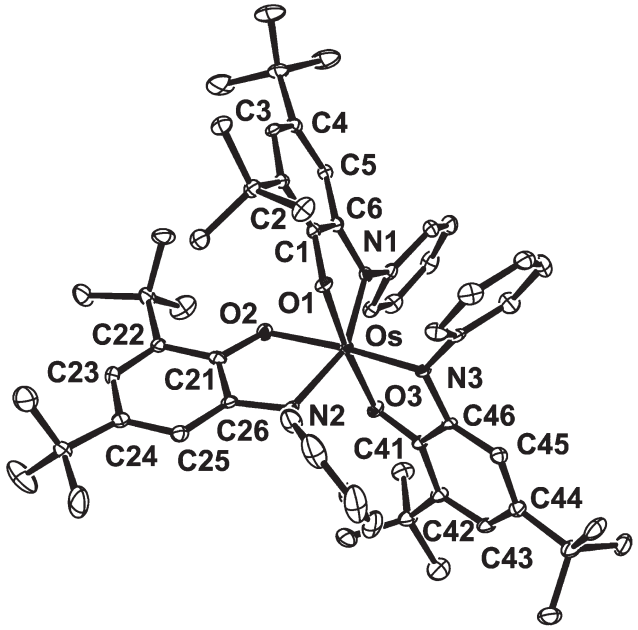

Fig. 1 Molecular structure of **4** in the crystal.

Table 1 Bond lengths in compound **4** (see Fig. 1)

	d/Å
Os–N1	1.986(3)
Os–N2	2.024(3)
Os–N3	1.940(3)
Os–O1	1.994(2)
Os–O2	2.027(2)
Os–O3	2.026(2)
O1–C1	1.323(4)
O2–C21	1.315(4)
O3–C41	1.330(4)
N1–C6	1.385(4)
N2–C26	1.376(4)
N3–C46	1.390(4)
C1–C2	1.423(4)
C2–C3	1.379(5)
C3–C4	1.417(5)
C4–C5	1.376(5)
C5–C6	1.411(5)
C6–C1	1.413(5)
C21–C22	1.411(5)
C22–C23	1.382(5)
C23–C24	1.415(5)
C24–C25	1.371(5)
C25–C26	1.412(4)
C26–C21	1.415(5)
C41–C42	1.423(4)
C42–C43	1.387(5)
C43–C44	1.415(5)
C44–C45	1.380(4)
C45–C46	1.403(4)
C46–C41	1.403(4)

configuration *mer*-MO_3N_3 at the metal centres (Fig. 1), selected bond angles are listed in Table S2.† The essential bond length parameters (Table 1) for the assignment of the ligand oxidation state in **4** have averaged values of 1.32 Å for C–O (range from 1.315(4)–1.330(4) Å), 1.38 Å for C–N (range from 1.376(4)–1.390(4) Å), and 1.38 Å for the revealing[23] C–C(*meta*) bonds within the six-membered ring (range from 1.371(5)–1.387(5) Å). These values seem to suggest a semiquinone assignment as the most appropriate[24] formulation for both **3** and **4**. Application of a recently published[10b] empirical correlation between metric parameters and the oxidation state of quinone-type ligands like Q_x yielded MOS (metric oxidation state) values of −1.40, −1.34 and −1.52 for the new **4** = $Os(Q_x)_3$. The average of −1.42 indicates a mixed iminosemiquinone (−1.0)/amidophenolate (−2.0) situation with slightly more semiquinone contribution.

Table 2 Redox potentials of the complexes

	$E_{1/2}$/V (ΔE_p/mV) *vs.* $Fc^{0/+a}$			
Complex	ox1	ox2	red1	red2
1[a]	+0.35(94)	+0.96(104)	−0.50(105)	−1.13(115)
2[a]	+0.51(81)	+1.17[c]	−0.45(103)	−1.20(94)
3[b]	−0.30(100)	+0.40(100)	−1.14(100)	(−1.91)[d]
4[a]	−0.16(60)	+0.60(60)	−1.23(60)	−2.00(60)

[a] CH_2Cl_2/0.1 M Bu_4NPF_6, 100 mV s^{-1}, 295 K. [b] CH_3CN/0.1 M Et_4NClO_4, 100 mV s^{-1}, 295 K, from ref. 6; potentials recalculated from SCE reference. [c] Peak potential for an irreversible process. [d] Not fully reversible.

The previously reported electrochemistry[4,5] of **1** and **2** has been confirmed by cyclic voltammetry in CH_2Cl_2/0.1 M Bu_4NPF_6. The voltammograms are given in Fig. S1† and the results are summarised in Table 2. The complexes undergo two one-electron oxidation and two one-electron reduction processes. The second oxidation step was found to be irreversible for **2**, as was the second reduction of **3**,[6] confirmed by the spectroelectrochemical experiments.

Like for the ruthenium complex pair **1″**/**3″**, the potentials are shifted by an average of about 0.7 V to lower values when going from the osmium/quinone compound **2″** to the monoiminoquinone analogue **4″**. In agreement with the N/O electronegativity difference, the monoiminoquinone systems are easier to oxidise but harder to reduce. The separation of potentials leads to large comproportionation constants K_c between 10^{10} and 10^{13} for the paramagnetic monocations and monoanions ($K_c = \exp(\Delta E \times nF/RT)$).[25]

EPR spectroscopy

X-band EPR measurements were done for the one-electron oxidised and reduced species, following electrochemical generation *in situ*. Spectra are shown in Fig. 2, 3, S2 and S3,† the data for the cation and anion complexes are listed in Table 3. No evidence for higher spin states has been found, we therefore assume doublet ground states resulting from antiferromagnetic spin–spin coupling.

One-electron oxidation of **1** results in the appearance of an isotropic EPR signal at g_{iso} = 1.991 at 295 K (Fig. 2 (top)), and in glassy frozen solution at 110 K appreciable *g* component splitting is observed with g_1 = 2.004, g_2 = 1.991 and g_3 = 1.977 (Fig. 2 (bottom); Table 3). Both the isotropic *g* factor of $\mathbf{1}^+$ (which is close to the value of 2.0023 for the free electron) and the relatively small $\Delta g = g_1 - g_3 = 0.027$ suggest a ligand-localised singly occupied MO (SOMO) with rather marginal contributions from the metal,[26] as supported by DFT spin density

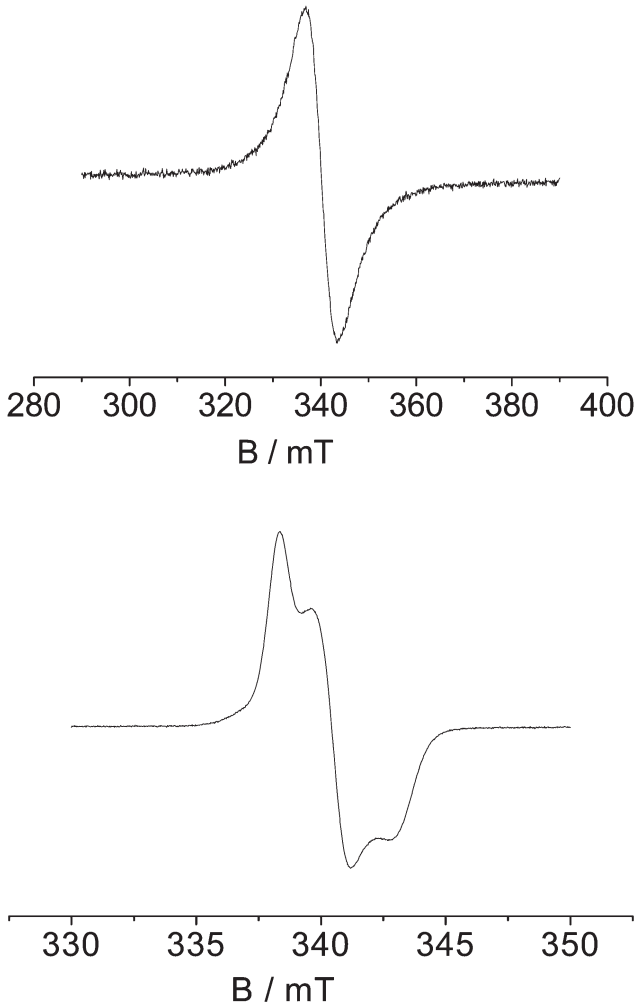

Fig. 2 X-band EPR spectra of electrochemically generated $\mathbf{1}^+$ at 295 K (top) and at 110 K (bottom) in CH_2Cl_2/0.1 M Bu_4NPF_6.

calculations (Fig. 4, *vide infra*). The electrochemically generated one-electron oxidised species $\mathbf{2}^+$ exhibits an unresolved EPR signal at 100 K (Fig. S2†); no signal was observed at 295 K. The *g* anisotropy could not be determined ($\Delta g < 0.06$) because of the broad signal with a peak-to-peak linewidth of nearly 10 mT. The higher g_{av} value of the osmium analogue $\mathbf{2}^+$ as compared to the result for the ruthenium radical $\mathbf{1}^+$ reflects the stronger spin–orbit coupling of the osmium system,[27] as do the broadness of the signal and its non-observability at ambient temperature.[28] However, the data are still compatible with predominantly ligand-centred spin – a notion which is confirmed by the Mulliken spin densities as calculated by DFT. Oxidation of the iminoquinone complexes to $\mathbf{3}^{+6}$ and $\mathbf{4}^+$ yields unresolved EPR signals (Fig. 3) with *g* factors close to 2 which suggests even less metal contribution.

The small *g* anisotropy in the EPR spectrum of $\mathbf{4}^+$, below the limits of X band EPR for the given linewidth, compares with the rather large splitting ($g_1 = 2.160$, $g_2 = 1.913$, $g_3 = 1.790$) for the osmium(II) complex $[Os(Q_x)(bpy)_2]^+$ with only one $Q_x^{\cdot -}$ semiquinone radical ligand.[27]

Fig. 4 (left) shows that the DFT calculated spin density in $\mathbf{1}^+$ is mainly localised on the Q ligands. ADF/BP calculations yield

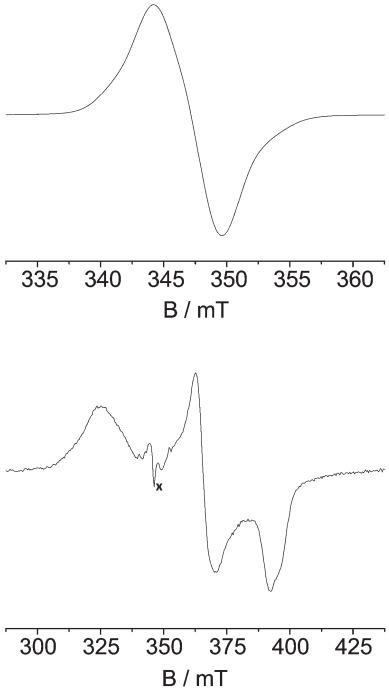

Fig. 3 X-band EPR spectra of electrochemically generated $\mathbf{4}^+$ (top) and $\mathbf{4}^-$ (bottom) at 110 K in CH_2Cl_2/0.1 M Bu_4NPF_6 (x: cavity signal).

Table 3 EPR data of complexes $\mathbf{1}^n$–$\mathbf{4}^n$ ($n = -, +$)

Complex[a]	*g* (at 295 K)	*g* (110 K)	Δg[b]	g_{av}[c]
$\mathbf{1}^+$	1.991	$g_1 = 2.004$ $g_2 = 1.991$ $g_3 = 1.977$	0.027	1.991
$\mathbf{1}^-$	Very weak signal	$g_1 = 2.041$ $g_2 = g_3 = 1.990$	0.05	2.007
$\mathbf{2}^+$	n.o.	2.027	<0.06	2.027
$\mathbf{2}^-$	n.o.	n.o.	—	—
$\mathbf{3}^{+d}$	1.9945	1.9945	<0.02	1.9945
$\mathbf{3}^{-d}$	2.0018	$g_1 = 2.0455$ $g_2 = 1.994$ $g_3 = 1.973$	0.073	2.006
$\mathbf{4}^+$	2.001	1.995	<0.03	1.995
$\mathbf{4}^-$	n.o.	$g_1 = 2.128$ $g_2 = 1.893$ $g_3 = 1.767$	0.361	1.935

[a] In CH_2Cl_2/0.1 M Bu_4NPF_6. [b] $\Delta g = g_1 - g_3$. [c] $g_{av} = [(g_1^2 + g_2^2 + g_3^2)/3]^{1/2}$. [d] From ref. 6.

spin densities of 0.405 for each Q and −0.215 for Ru. This is further confirmed by the ADF/BP calculated isotropic *g* factor value of 2.005 which is in reasonable agreement with the experimental *g* factor value of 1.991 (see Table 3). The calculations of the osmium analogue $\mathbf{2}^+$ indicate even less metal participation with spin densities of 0.323 for each Q and 0.032 for Os; the calculated *g* factor at $g_{iso} = 1.996$ is smaller than the experimental value at 2.027. However, the calculated Δg at 0.04 is in accordance with the observations (Table 3).

One-electron reduction of complex **1** results in a signal (Fig. S3) with $g_1 = 2.041$ and $g_2 = g_3 = 1.990$ in glassy frozen CH_2Cl_2 solution at 110 K. Only a very weak signal is observed at 295 K. The *g* anisotropy $\Delta g = 0.05$, suitable to evaluate the

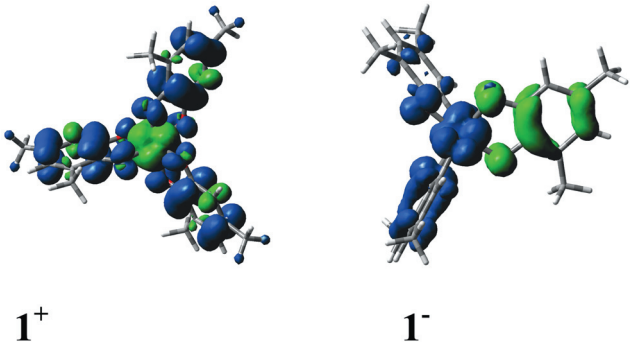

Fig. 4 DFT calculated spin densities of $\mathbf{1}^{+}$ (left) and $\mathbf{1}^{-}$ (right). Blue areas indicate positive and green areas negative spin densities.

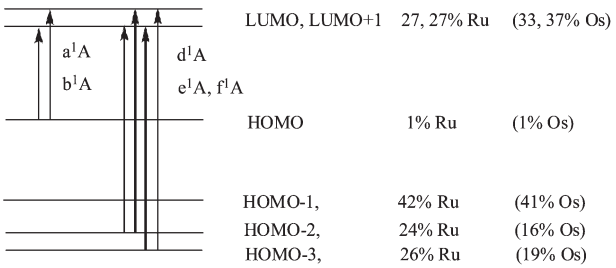

Fig. 5 The qualitative MO scheme of complexes **1** (Ru) and **2** (Os). Arrows indicate the main contributions to the lowest allowed TD-DFT calculated transitions.

amount of spin on the heavy metal,[26] indicates significant ruthenium contribution to the SOMO. These results point to a metal–ligand mixed-spin intermediate $\mathbf{1}^{-}$, in agreement with the DFT calculation results (Fig. 4). No EPR signal was observed at 295 K and at 110 K for the electrochemically generated one-electron reduced osmium species $\mathbf{2}^{-}$. Reduction of the iminoquinone complexes to $\mathbf{3}^{-6}$ and $\mathbf{4}^{-}$ produces EPR signals (Fig. 3) with sizeable *g* factor anisotropy (Table 3), indicating considerable metal contributions to the SOMO. The large difference in Δg between the Ru and Os analogues is well understood[27] in terms of the large differences of spin–orbit coupling constants. The larger orbital splitting expected for the iminoquinone compounds is probably responsible for the better observability of EPR signals due to slower relaxation.

According to DFT calculations the electron is accepted in the course of the reduction by the set of almost degenerate LUMO and LUMO + 1 orbitals with approximately 27% or 37% contribution from the metal in $\mathbf{1}^{-}$ or $\mathbf{2}^{-}$, respectively (Fig. 5). The ADF/BP calculations give averaged spin densities of 0.480 for Ru and of 0.173 for each Q ligand in the case of $\mathbf{1}^{-}$, and of 0.622 for Os and of 0.126 for each Q ligand in the case of $\mathbf{2}^{-}$.

Remarkably, no evidence for spin hopping (such as temperature-dependent EPR line broadening[29,30]) has been observed here, suggesting spin delocalisation on the EPR time scale of about 10^{-8} s.

UV-vis-NIR spectroelectrochemistry

In order to obtain more information on the electronic distribution in various accessible redox states, the UV-vis-NIR

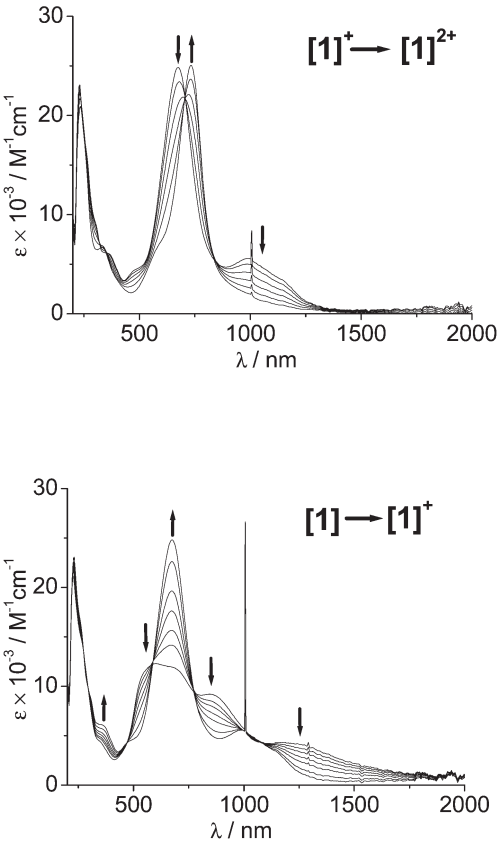

Fig. 6 UV-vis-NIR spectroelectrochemistry of the conversion $\mathbf{1}^{(0)\rightarrow(+)}$ (bottom) and $\mathbf{1}^{(+)\rightarrow(2+)}$ (top) in CH_2Cl_2/0.1 M Bu_4NPF_6.

spectroelectrochemical changes of the complexes **1**, **2** and **4** were monitored using an OTTLE cell (Fig. 6–9 and S5†).[12] The data, including reported values for $\mathbf{3}''$,[6] are summarised in Table 4.

The neutral compound **1** exhibits near infrared (NIR) absorption with a band maximum at 1220 nm, in addition to several shoulders and a broad band maximum at 585 nm (Fig. 6).[11] For the osmium analogue **2**, the band maximum in the NIR absorption region is blue-shifted to 990 nm and several shoulders, with a band maximum at 596 nm, are observed (Fig. 7, Table 4). Corresponding bands of **4** lie at λ_{max} = 925 and 505 nm. TD-DFT calculations including solvent effect incorporation can be used to assign transitions in the experimental spectra of neutral complexes **1** and **2**, as shown in Tables 5 and 6, respectively.

The dominant excitations contributing to the two lowest lying transitions in the visible region are schematically depicted in Fig. 5. Fig. 5 shows the qualitative MO scheme of **1**, corresponding frontier orbitals are depicted in Fig. S4.† The calculations slightly underestimate the energy of the lowest lying transition of **1** found at 1220 nm (calculated at 1350 nm). This transition can be characterised as mixed LMCT/LLCT excitation from the ligand-based HOMO (Fig. S4†) into the set of LUMOs. The intense band around 687 nm is reasonably reproduced by TD-DFT calculations and is attributed to mixed MLCT/LLCT transitions from the HOMO − 2 and HOMO − 3 to the LUMO and LUMO + 1. TD-DFT calculations reproduce the shift of excitations to higher energy when going from **1** to **2**.

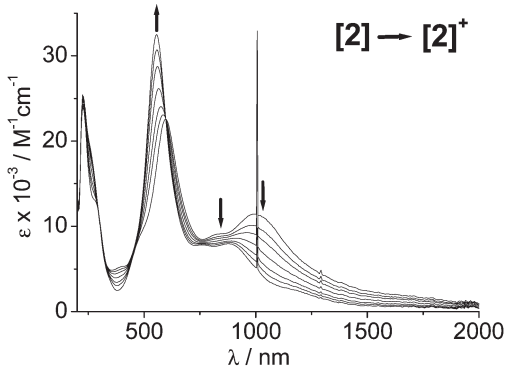

Fig. 7 UV-vis-NIR spectroelectrochemistry of the conversion $\mathbf{2}^{(0)\rightarrow(+)}$ in CH_2Cl_2/0.1 M Bu_4NPF_6.

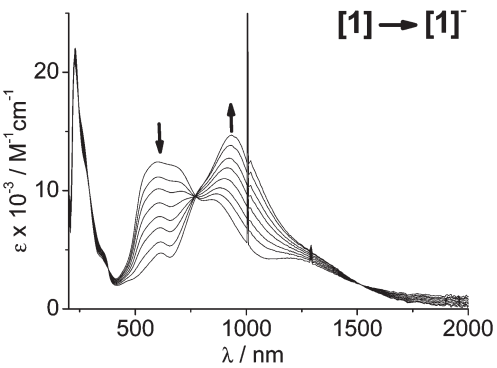

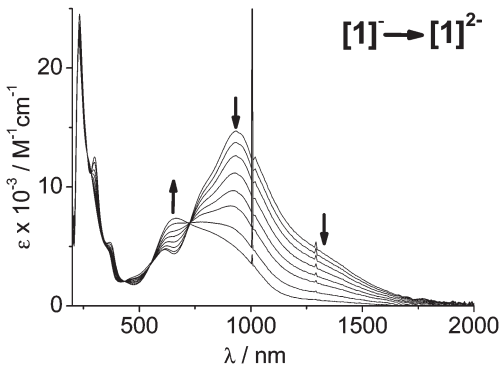

Fig. 8 UV-vis-NIR spectroelectrochemistry of the conversion $\mathbf{1}^{(0)\rightarrow(-)}$ (top) and $\mathbf{1}^{(-)\rightarrow(2-)}$ (bottom) in CH_2Cl_2/0.1 M Bu_4NPF_6.

Oxidation produces monocations with higher energy absorptions than those of the neutral precursors. The bands around 673 nm and 990 nm for $\mathbf{1}^+$ (Fig. 6) and at 555 nm and 882 nm for $\mathbf{2}^+$ (Fig. 7) are assigned as semiquinone-to-quinone, *i.e.* ligand-to-ligand intervalence charge transfer (LLIVCT) transitions, in agreement with a preferential ligand-based oxidation, as suggested by EPR. Both complexes show a decrease in NIR band intensity on the first oxidation, and the NIR absorption disappears after the second oxidation in the system $\mathbf{1}^{n+}$ (Fig. 6 (top)). For the dicationic state $\mathbf{1}^{2+}$, the previous HOMO is now empty and no transition can occur from this level; an

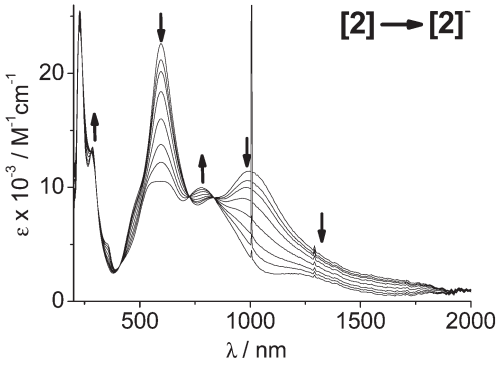

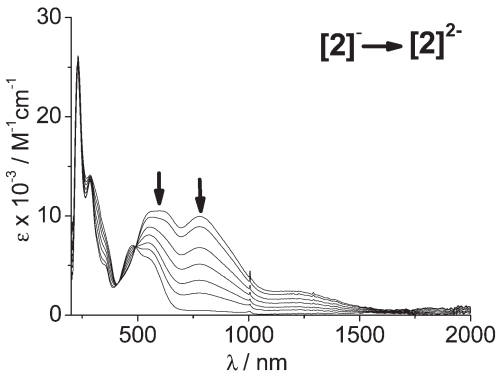

Fig. 9 UV-vis-NIR spectroelectrochemistry of the conversion $\mathbf{2}^{(0)\rightarrow(-)}$ (top) and $\mathbf{2}^{(-)\rightarrow(2-)}$ (bottom) in CH_2Cl_2/0.1 M Bu_4NPF_6.

Table 4 Absorption data[a]

Complex	λ_{max}/nm (ε/M^{-1} cm^{-1})
$\mathbf{1}^{2+}$	334 (6800), 735 (25 200)
$\mathbf{1}^{+}$	365 (sh), 673 (24 900), 990 (5600), 1100 (sh)
$\mathbf{1}^{0}$	585 (12 300), 687 (sh), 860 (9200), 1220 (4300)
$\mathbf{1}^{-}$	614 (4800), 770 (sh), 932 (14 700), 1300 (sh)
$\mathbf{1}^{2-}$	300 (12 600), 368 (5400), 660 (7300), 850 (sh)
$\mathbf{2}^{+}$	555 (32 500), 765 (7800), 882 (7900), 1180 (sh)
$\mathbf{2}^{0}$	596 (22 600), 830 (sh), 990 (11 500)
$\mathbf{2}^{-}$	590 (10 500), 780 (10 000), 1210 (2400)
$\mathbf{2}^{2-}$	478 (7000), 550 (sh)
$\mathbf{3}^{2+}$	503 (sh), 584 (23 000), 770 (14 500)
$\mathbf{3}^{+}$	437 (9900), 604 (22 400), 837 (7300), 925 (6900), >2000
$\mathbf{3}$	332 (14 100), 553 (15 600), 725 (9600), 1278 (5500)
$\mathbf{3}^{-}$	490 (7200), 567 (6400), 817 (17 400), 1000 (sh)
$\mathbf{4}^{2+}$	385 (sh), 526 (10 700), 645 (sh), 795 (sh), 882 (6600), 1580 (400)
$\mathbf{4}^{+}$	509 (11 800), 655 (4100), 800 (sh), 865 (4070), 970 (sh), 1310 (560), 1730 (600)
$\mathbf{4}^{0}$	320 (sh), 505 (8000), 650 (sh), 925 (4500)
$\mathbf{4}^{-}$	295 (sh), 467 (4700), 533 (4600), 658 (7000), 760 (sh), 1450 (540)
$\mathbf{4}^{2-}$	295 (sh), 340 (sh), 473 (4500), 629 (4500)

[a] From spectroelectrochemistry in CH_2Cl_2/0.1 M Bu_4NPF_6.

MLCT-type transition remains for the lowest-lying absorption as shown previously for the related $\mathbf{3}^{2+}$,[6] and as adopted here also for the accessible $\mathbf{4}^{2+}$.

Reduction of the complexes to $\mathbf{1}^-$ (Fig. 8), $\mathbf{2}^-$ (Fig. 9), $\mathbf{3}^-$,[6] or $\mathbf{4}^-$ (Fig. S5†) results in the diminishing of the long-wavelength NIR intensity and the appearance of intense bands at 658 nm

Table 5 Selected G03/PBE0/CPCM calculated lowest allowed TD-DFT singlet transitions for complex **1**

State	Main character (in %)	Calculated		Experiment
		Transition energy[a]	Oscillator strength	$\lambda_{max}/\varepsilon$[b]
a^1A	85 (HOMO → LUMO)	0.90 (1375)	0.083	
b^1A	91 (HOMO → LUMO + 1)	1.04 (1350)	0.082	1220/4300
c^1A	Mixed (HOMO − 2, HOMO − 3 → LUMO, LUMO + 1)	1.44 (858)	0.003	860/9200
d^1A	Mixed (HOMO − 2, HOMO − 3 → LUMO, LUMO + 1)	1.94 (639)	0.329	
e^1A	Mixed (HOMO − 2, HOMO − 3 → LUMO, LUMO + 1)	1.97 (631)	0.315	687 sh
e^1A	Mixed (HOMO − 4, HOMO − 5 → LUMO, LUMO + 1)	2.27 (547)	0.064	
g^1A	Mixed (HOMO − 4, HOMO − 5 → LUMO, LUMO + 1)	2.29 (541)	0.042	585/12 300

[a] Transition energies in eV (or wavelengths in nm). [b] Absorption maxima in nm, molar extinction coefficients in M^{-1} cm^{-1}.

Table 6 Selected G03/PBE0/CPCM calculated lowest allowed TD-DFT singlet transitions for complex **2**

State	Main character (in %)	Calculated		Experiment
		Transition energy[a]	Oscillator strength	$\lambda_{max}/\varepsilon$[b]
a^1A	96 (HOMO → LUMO)	1.18 (1050)	0.079	
b^1A	91 (HOMO → LUMO + 1)	1.21 (1027)	0.085	990/11 500
c^1A	Mixed (HOMO − 2, HOMO − 3 → LUMO, LUMO + 1)	1.68 (738)	0.003	830 sh
d^1A	Mixed (HOMO − 2, HOMO − 3 → LUMO, LUMO + 1)	2.11 (585)	0.330	
e^1A	Mixed (HOMO − 2, HOMO − 3 → LUMO, LUMO + 1)	2.16 (573)	0.309	596/22 600
f^1A	70 (HOMO − 3 → LUMO + 1)	2.25 (551)	0.087	

[a] Transition energies in eV (or wavelengths in nm). [b] Absorption maxima in nm, molar extinction coefficients in M^{-1} cm^{-1}.

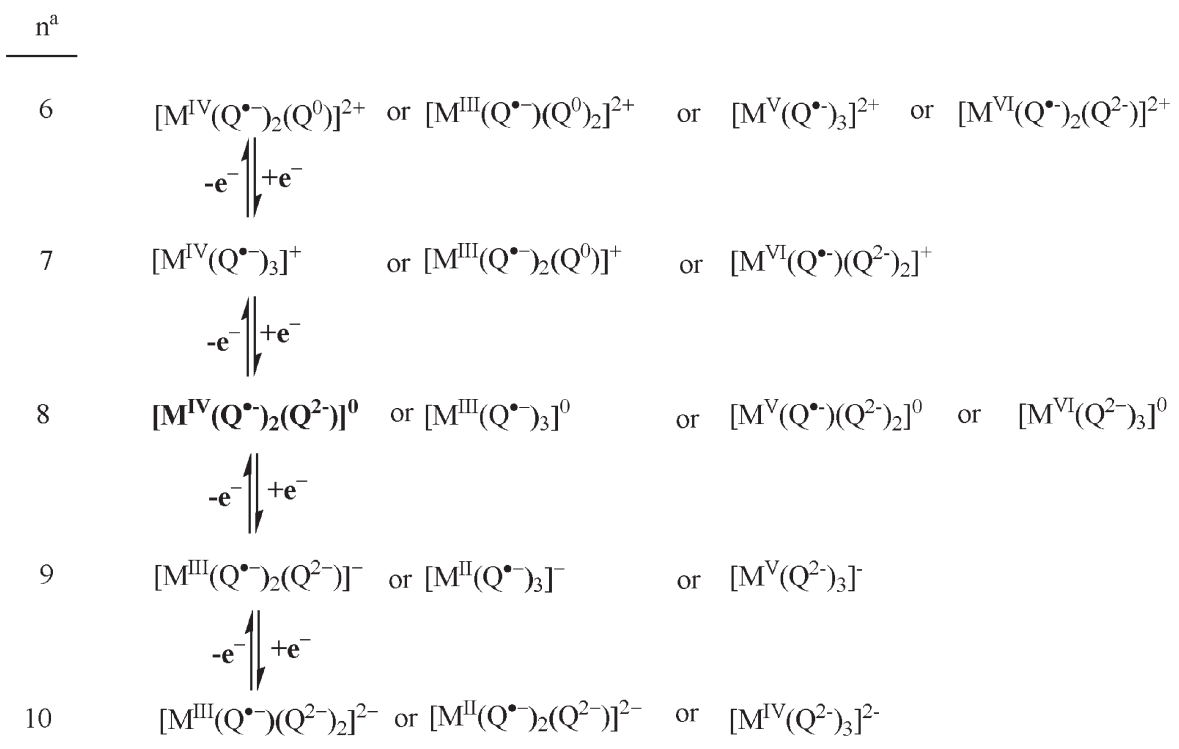

[a] n = m + p: Sum of electrons from the metal (d^m configuration) and the ligand, $(\pi^*)^p$.

Scheme 1 Alternative formulations for the oxidised and reduced states of $[M(Q)_3]$ (favoured descriptions on the left).

($\mathbf{4}^-$) and 932 nm ($\mathbf{1}^-$). Based on the EPR results and DFT calculations, they can be attributed to LMCT/MLCT mixed transitions which get diminished on second reduction.

Conclusions

As for a generalised assignment, both the DFT calculations (Fig. 4, 5 and S4†) and the Hückel MO approach for trigonal MQ_3 predict a HOMO with a node at the centre, *i.e.* without significant contributions from the metal, whereas the LUMO and LUMO + 1 are M/Q orbital mixed. EPR spectroscopy confirms this notion because metal contribution results in enhanced *g* shifts and *g* anisotropy as well as in shortened relaxation times and thus diminished signal observability at higher temperatures. All these effects are more pronounced for anions *vs.* cations, and for the osmium systems (**2″**, **4″**) with the higher spin–orbit coupling constant of the metal relative to Ru. The differences between the quinone and iminoquinone systems reflect a stronger orbital interaction for the mixed O/N donor ligand.

Orbital interaction differences are also responsible for the generally smaller electronic transition energies of the ruthenium analogues relative to the osmium species. In all four cases **1″–4″**, the neutral "native" states exhibit the most conspicuous long-wavelength absorption features (Table 4). In agreement with reviewed concepts[31] for near infrared absorption, this result would be compatible with a semiquinonato radical-involving formulation $[M^{IV}(Q^{\cdot-})_2(Q^{2-})]$, as favoured also by the structural correlation analysis (*vide supra*).

The favoured oxidation state description for the monocations as given in Scheme 1 is the $[M^{III}(Q^{\cdot-})_2(Q^0)]^+$ formulation, resulting through electron removal from a ligand-based HOMO and involving a ↑↓↑ three-spin coupling pattern[32] with one ligand-based unpaired electron for the $(Q^{\cdot-})M^{III}(Q^{\cdot-})$ moiety. One-electron reduction produces anions **1**$^-$**–4**$^-$ with metal–ligand mixed spin, in agreement with the DFT calculations. The favoured oxidation state description for the monoanions according to Scheme 1 is $[M^{III}(Q^{\cdot-})_2(Q^{2-})]^-$ with a minor contribution from the all-ligand spin formulation $[M^{II}(Q^{\cdot-})_3]^-$. In spite of the ligand-based mixed valency necessitated by the oxidation and reduction processes, we could not detect long-wavelength (λ_{max} > 1000 nm) near infrared absorbance for the electrogenerated ions studied here. Such ligand-to-ligand intervalence charge transfer (LL′IVCT) bands[1c,31] may be very broad, low in intensity and/or occurring at unusually low energies.[33]

Acknowledgements

This work has been supported by the Deutsche Forschungsgemeinschaft, by the Fonds der Chemischen Industrie and by the European Union (COST D35 and CM1002). S.Z. thanks the Ministry of Education of the Czech Republic (grant LD11086) for support.

References

1 (*a*) C. K. Jørgensen, *Coord. Chem. Rev.*, 1966, **1**, 164; (*b*) M. D. Ward and J. A. McCleverty, *J. Chem. Soc., Dalton Trans.*, 2002, 275; (*c*) P. Chaudhuri, C. N. Verdani, E. Bill, E. Bothe, T. Weyhermüller and K. Wieghardt, *J. Am. Chem. Soc.*, 2001, **123**, 2213; (*d*) W. Kaim, *Eur. J. Inorg. Chem.*, 2012, 343; (*e*) Forum Issue on Redox Non-Innocent Ligands: *Inorg. Chem.*, 2011, **50**, 9737

2 (*a*) C. G. Pierpont and R. M. Buchanan, *Coord. Chem. Rev.*, 1981, **38**, 45; (*b*) C. G. Pierpont and C. W. Lange, *Progr. Inorg. Chem.*, 1994, **41**, 331; (*c*) C. G. Pierpont, *Coord. Chem. Rev.*, 2001, **219–221**, 415; (*d*) C. G. Pierpont, *Inorg. Chem.*, 2011, **50**, 9766.

3 (*a*) M. Haga, E. S. Dodswort and A. B. P. Lever, *Inorg. Chem.*, 1986, **25**, 447; (*b*) A. B. P. Lever, P. R. Auburn, E. S. Dodsworth, M. Haga, W. Liu, M. Melnik and W. A. Nevin, *J. Am. Chem. Soc.*, 1988, **110**, 8076; (*c*) S. Ernst, P. Hänel, J. Jordanov, W. Kaim, V. Kasack and E. Roth, *J. Am. Chem. Soc.*, 1989, **111**, 1733.

4 (*a*) P. Zanello and M. Corsini, *Coord. Chem. Rev.*, 2006, **250**, 2000; (*b*) R. R. Kapre, E. Bothe, T. Weyhermüller, S. DeBeer George, N. Muresan and K. Wieghardt, *Inorg. Chem.*, 2007, **46**, 7827; (*c*) T. B. Karpishin, M. S. Gebhard, E. I. Solomon and K. N. Raymond, *J. Am. Chem. Soc.*, 1991, **113**, 2977.

5 S. Bhattacharya, S. R. Boone, G. A. Fox and C. G. Pierpont, *J. Am. Chem. Soc.*, 1990, **112**, 1088.

6 D. Das, A. K. Das, B. Sarkar, T. K. Mondal, S. M. Mobin, J. Fiedler, S. Záliš, F. A. Urbanos, R. Jiménez-Aparicio, W. Kaim and G. K. Lahiri, *Inorg. Chem.*, 2009, **48**, 11853.

7 (*a*) C. Remenyi and M. Kaupp, *J. Am. Chem. Soc.*, 2005, **127**, 11399; (*b*) D. Kalinina, C. Dares, H. Kaluarachchi, P. G. Potvin and A. B. P. Lever, *Inorg. Chem.*, 2008, **47**, 10110.

8 (*a*) S. Patra, B. Sarkar, S. M. Mobin, W. Kaim and G. K. Lahiri, *Inorg. Chem.*, 2003, **42**, 6469; (*b*) D. Das, B. Sarkar, D. Kumbhakar, T. K. Mondal, S. M. Mobin, J. Fiedler, F. A. Urbanos, R. Jiménez-Aparicio, W. Kaim and G. K. Lahiri, *Chem.–Eur. J.*, 2011, **17**, 11030.

9 (*a*) J. L. Boyer, J. Rochford, M.-K. Tsai, J. T. Muckerman and E. Fujita, *Coord. Chem. Rev.*, 2010, **254**, 309; (*b*) S. Ghosh and M.-H. Baik, *Angew. Chem.*, 2012, **124**, 1247, (*Angew. Chem., Int. Ed.*, 2012, **51**, 1221).

10 (*a*) A. I. Poddel'sky, V. K. Cherkasov and G. A. Abakumov, *Coord. Chem. Rev.*, 2009, **253**, 291; (*b*) S. N. Brown, *Inorg. Chem.*, 2012, **51**, 1251.

11 Y. Sasaki and M. Abe, *Chem. Record*, 2004, **4**, 279.

12 M. Krejčik, M. Danek and F. Hartl, *J. Electroanal. Chem. Interfacial Electrochem.*, 1991, **317**, 179.

13 W. Kaim, S. Ernst and V. Kasack, *J. Am. Chem. Soc.*, 1990, **112**, 173.

14 G. M. Sheldrick, *SHELXS97*, University of Göttingen, Göttingen, Germany, 1997.

15 M. J. Frisch, G. Trucks, H. B. Schlegel, G. E. Scuseria, M. A. Robb, J. R. Cheeseman, J. A. Montgomery Jr., T. Vreven, K. N. Kudin, J. C. Burant, J. M. Millam, S. S. Iyengar, J. Tomasi, V. Barone, B. Mennucci, M. Cossi, G. Scalmani, N. Rega, G. A. Petersson, H. Nakatsuji, M. Hada, M. Ehara, K. Toyota, R. Fukuda, J. Hasegawa, M. Ishida, T. Nakajima, Y. Honda, O. Kitao, H. Nakai, M. Klene, X. Li, J. E. Knox, H. P. Hratchian, J. B. Cross, V. Bakken, C. Adamo, J. Jaramillo, R. Gomperts, R. E. Stratmann, O. Yazyev, A. J. Austin, R. Cammi, C. Pomelli, J. W. Ochterski, P. Y. Ayala, K. Morokuma, G. A. Voth, P. Salvador, J. J. Dannenberg, V. G. Zakrzewski, S. Dapprich, A. D. Daniels, M. C. Strain, O. Farkas, D. K. Malick, A. D. Rabuck, K. Raghavachari, J. B. Foresman, J. V. Ortiz, Q. Cui, A. G. Baboul, S. Clifford, J. Cioslowski, B. B. Stefanov, G. Liu, A. Liashenko, P. Piskorz, I. Komaromi, R. L. Martin, D. J. Fox, T. Keith, M. A. Al-Laham, C. Y. Peng, A. Nanayakkara, M. Challacombe, P. M. W. Gill, B. Johnson, W. Chen, M. W. Wong, C. Gonzalez and J. A. Pople, *GAUSSIAN 03 (Revision C.02)*, Gaussian, Inc., Wallingford, CT, 2004.

16 (*a*) G. te Velde, F. M. Bickelhaupt, S. J. A. van Gisbergen, C. Fonseca Guerra, E. J. Baerends, J. G. Snijders and T. Ziegler, *J. Comput. Chem.*, 2001, **22**, 931; (*b*) ADF2010.01, SCM, Theoretical Chemistry, Vrije Universiteit, Amsterdam, The Netherlands, http://www.scm.com

17 J. P. Perdew, K. Burke and M. Ernzerhof, *Phys. Rev. Lett.*, 1996, **77**, 3865.

18 P. C. Hariharan and J. A. Pople, *Theor. Chim. Acta*, 1973, **28**, 213.

19 D. Andrae, U. Haussermann, M. Dolg, H. Stoll and H. Preuss, *Theor. Chim. Acta*, 1990, **77**, 123.

20 M. Cossi, N. Rega, G. Scalmani and V. Barone, *J. Comput. Chem.*, 2003, **24**, 669.

21 (*a*) A. D. Becke, *Phys. Rev. A*, 1988, **38**, 3098; (*b*) J. P. Perdew and Y. Wang, *Phys. Rev. B*, 1992, **45**, 13244.

22 (*a*) E. van Lenthe, A. van der Avoird and P. E. S. Wormer, *J. Chem. Phys.*, 1997, **107**, 2488; (*b*) E. van Lenthe, A. van der Avoird and P. E. S. Wormer, *J. Chem. Phys.*, 1998, **108**, 4783.

23 S. Samanta, P. Singh, J. Fiedler, S. Záliš, W. Kaim and S. Goswami, *Inorg. Chem.*, 2008, **47**, 1625.
24 S. Bhattacharya, P. Gupta, F. Basuli and C. G. Pierpont, *Inorg. Chem.*, 2002, **41**, 5810.
25 C. Creutz, *Prog. Inorg. Chem.*, 1983, **30**, 1.
26 W. Kaim, *Inorg. Chem.*, 2012, **50**, 9752.
27 S. Ye, B. Sarkar, C. Duboc, J. Fiedler and W. Kaim, *Inorg. Chem.*, 2005, **44**, 2843.
28 M. Heilmann, S. Frantz, W. Kaim, J. Fiedler and C. Duboc, *Inorg. Chim. Acta*, 2006, **359**, 821.
29 M. Heilmann, F. Baumann, W. Kaim and J. Fiedler, *J. Chem. Soc., Faraday Trans.*, 1996, **92**, 4227.
30 M. K. DeArmond, K. W. Hanck and D. W. Wertz, *Coord. Chem. Rev.*, 1985, **64**, 65.
31 W. Kaim, *Coord. Chem. Rev.*, 2011, **255**, 2503.
32 S. Ye, B. Sarkar, F. Lissner, T. Schleid, J. van Slageren, J. Fiedler and W. Kaim, *Angew. Chem.*, 2005, **117**, 2140, (*Angew. Chem., Int. Ed.*, 2005, **44**, 2103).
33 S. Kämper, A. Paretzki, J. Fiedler, S. Záliš and W. Kaim, *Inorg. Chem.*, 2012, **51**, 2097.